

FlexiReID: Adaptive Mixture of Expert for Multi-Modal Person Re-Identification

Zhen Sun^{*1}, Lei Tan^{*2}, Yunhang Shen³, Chengmao Cai¹, Xing Sun³, Pingyang Dai^{†1}, Liujuan Cao¹, Rongrong Ji^{1,4}

¹Key Laboratory of Multimedia Trusted Perception and Efficient Computing, Ministry of Education of China, Xiamen University, 361005, P.R. China.

²National University of Singapore.

³Tencent YouTu Lab.

⁴Institute of Artificial Intelligence, Xiamen University, Xiamen, China

Abstract

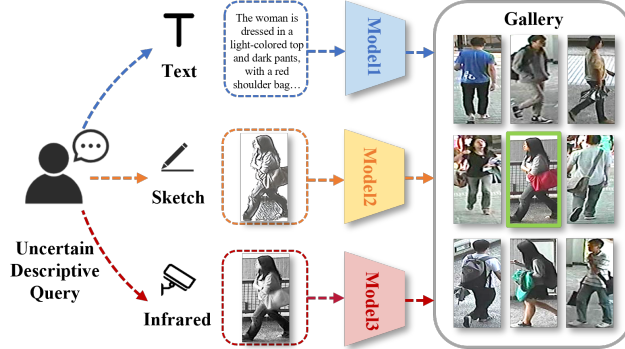
Multimodal person re-identification (Re-ID) aims to match pedestrian images across different modalities. However, most existing methods focus on limited cross-modal settings and fail to support arbitrary query-retrieval combinations, hindering practical deployment. We propose FlexiReID, a flexible framework that supports seven retrieval modes across four modalities: rgb, infrared, sketches, and text. FlexiReID introduces an adaptive mixture-of-experts (MoE) mechanism to dynamically integrate diverse modality features and a cross-modal query fusion module to enhance multimodal feature extraction. To facilitate comprehensive evaluation, we construct CIRS-PEDES, a unified dataset extending four popular Re-ID datasets to include all four modalities. Extensive experiments demonstrate that FlexiReID achieves state-of-the-art performance and offers strong generalization in complex scenarios.

1 Introduction

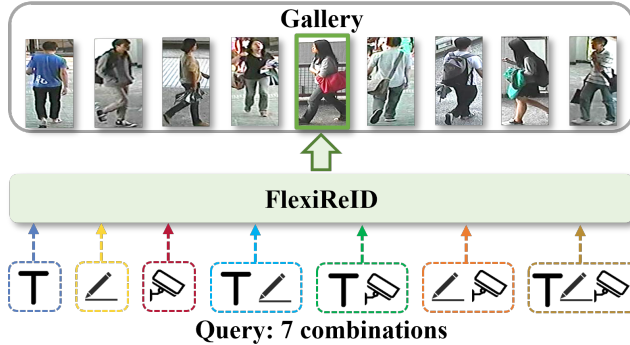
Pedestrian re-identification (ReID) is a critical technology in computer vision, focused on matching individuals across different camera viewpoints. This capability is essential for various surveillance and security operations, leading to diverse applications in fields such as security, urban management, retail, and law enforcement. ReID tasks are classified into single-modal ReID and cross-modal ReID. Single-modal ReID focuses on retrieval between RGB images, depending on the extraction and matching of visual features. However, it encounters several challenges in practical applications, including

^{*}Equal contribution.

[†]Corresponding author.



(a) Existing Methods



(b) Our Method

Figure 1: Illustration of our idea. Existing cross-modal ReID models primarily address single-modality retrieval, which limits their practical applicability. In contrast, our method enables flexible retrieval across seven different modality combinations. The green boxes match the query.

variations in lighting, occlusions, differences in viewpoints, and changes in pedestrian poses, all of which can compromise recognition accuracy and robustness. In contrast, cross-modal pedestrian re-identification (ReID) presents significant advantages. Unlike single-modal approaches, cross-modal ReID incorporates various modalities, including textual descriptions, infrared images, and sketches. By leveraging multimodal information, cross-modal ReID offers complementary features that sustain high recognition accuracy across diverse environmental conditions, such as lighting variations and nighttime scenarios, thereby improving the system's robustness and adaptability. For example, in low-light or nighttime conditions, infrared images can provide clearer outlines of pedestrians compared to RGB images, while textual descriptions and sketches can supply additional semantic and structural information when visual data is incomplete or ambiguous. However, existing cross-modal ReID, as shown in figure 1a, has an inherent limitation: it typically supports retrieval only between specific pairs of modalities, which restricts its ability to accommodate various combinations of modalities. In real-world scenarios, we often receive information from multiple modalities simultaneously. If retrieval is confined to a single modality paired with RGB images, the potential of existing mul-

timodal information remains underutilized. This raises a critical question: **Can we establish a unified cross-modal person re-identification framework that supports flexible retrieval across any combination of modalities?**

Based on this, we propose the FlexiReID framework, which spans four modalities (Text, Sketch, Infrared, RGB) and supports seven different combinations of multimodal retrieval: Text-to-RGB, Sketch-to-RGB, Infrared-to-RGB, Text+Sketch-to-RGB, Text+Infrared-to-RGB, Sketch+Infrared-to-RGB, and Text+Sketch+Infrared-to-RGB, as shown in figure1b. Inspired by CLIP, which is pre-trained on a large-scale dataset of 400 million image-text pairs, FlexiReID utilizes a simple dual-encoder architecture for the extraction of visual and textual features. Notably, the three visual modalities share a single image encoder. In order to efficiently extract features of diverse modalities, we introduce an Adaptive Expert Allocation Mixture of Experts (AEA-MoE) mechanism. Specifically, our proposed adaptive routing mechanism dynamically selects a varying number of expert combinations based on the attributes of the input features. Compared to the traditional Top-K routing mechanism, which selects a fixed number of experts, our approach better leverages the strengths of the multi-expert system, thereby optimizing the extraction of multi-modal features. Additionally, we designed a multi-modal feature fusion module called Cross-Modal Query Fusion (CMQF). This module accepts multi-modal feature inputs and uses learnable embedded features to compensate for missing modalities. Its superior feature fusion capability further enhances the flexible retrieval performance of FlexiReID. In this study, We introduce the concept of flexible retrieval to the field of person re-identification for the first time, pioneering a new research direction. The core idea of flexible retrieval is to accurately perform person retrieval using the existing modalities, even in the presence of missing modalities. To achieve this challenging objective, We expanded the modalities of the four datasets (CUHK-PEDES, ICFG-PEDES, RSTPReid, and SYSU-MM01), constructing a unified dataset named CIRS-PEDES, which encompasses four modalities: text, sketches, RGB images, and infrared images. Experimental results on the CIRS-PEDES show that the proposed FlexiReID outperforms several other state-of-the-art methods, demonstrating its flexibility and effectiveness in complex scenes. Our main contributions are summarized as follows:

- We introduce the concept of flexible retrieval in the field of person re-identification for the first time and propose FlexiReID, which supports flexible retrieval with arbitrary modality combinations, opening up a new research direction.
- In FlexiReID, we propose the AEA-MoE mechanism, which dynamically selects different numbers of experts based on the input features. Additionally, we design the CMQF module, which leverages learnable embedding features to compensate for missing modalities and fuse different modality features.
- We construct a unified dataset, CIRS-PEDES, which contains four modalities. Extensive experiments demonstrate the effectiveness of FlexiReID.

2 Related Work

2.1 Vision-Language Pre-Training Models

Vision-language pre-training models, pre-trained on image-text corpora, have demonstrated significant potential in downstream vision and language tasks, such as few-shot classification[1, 2, 3], cross-modality generation[4, 5, 6, 7], and visual recognition[8]. The pre-training approaches mainly contain the BERT-like masked-language and masked-region modeling methods[9, 10, 11, 12], contrastive learning for learning a joint embedding space of vision and language[13, 14, 15, 16, 17], and vision-language multimodal autoregressive techniques[18, 19]. In this paper, we focus on the contrastive vision-language models (VLMs) that adopt a dual encoder to encode images and texts into the joint embedding space and use contrastive learning to align the visual and textual representations. A representative work is CLIP[13], which aggregates 400 million image-text pairs from websites. It employs a dual-encoder architecture consisting of an image encoder and a text encoder, and showcases remarkable prompt-based zero-shot performance across diverse visual classification tasks by exploiting alignments between text and image features.

2.2 Cross-Modal Person Re-Identification

Person re-identification (ReID) focuses on retrieving all images of a specific pedestrian across different devices, with an emphasis on learning distinctive pedestrian features. Based on the various modalities used to represent pedestrian information, ReID can be divided into single-modal ReID[20, 21] and cross-modal ReID[22, 23, 24]. Cross-modal ReID, in particular, addresses unique situations where RGB images of pedestrians are not readily available. It suggests utilizing non-RGB modalities(such as infrared images[25, 26, 27], text descriptions[28, 29, 30], and sketches[22, 31, 32]) to represent pedestrian information, thereby broadening the application scope of ReID technology. Li et al.[33] first propose to explore the problem of retrieving the target pedestrians with natural language descriptions for adaptation to real-world circumstances. Shao et al.[30] analyze the granularity differences between the visual modality and textual modality and propose a granularity-unified representation learning method for text-based ReID. Pang et al.[34] first propose to use professional sketches as queries to search for the target person in the RGB gallery. They design cross-domain adversarial learning methods to mine domain-invariant feature representations. In order to explore the complementarity between the sketch modality and the text modality, Zhai et al.[35] introduce a multi-modal ReID task that combines both sketch and text modalities as queries for retrieval. However, existing methods are limited to retrieval between specific pairs of modalities and cannot be extended to support retrieval across various combinations of modalities, which fails to meet the demands of real-world scenarios. To address this limitation, we propose the FlexiReID framework, which spans four modalities and supports seven different combinations for multimodal retrieval.

2.3 Mixture-of-Experts

Mixture-of-Experts (MoE) has been extensively explored in computer vision[36], natural language processing[37], and vision-language pretraining[38]. MoE learns a series of expert networks and a gating network, where the outputs of the expert networks are weighted by gating scores generated by the gating network before the weighting operation. In more recent works, some researchers[39, 37, 40, 41] use the gating scores as a criterion to sparsely select only one or a few experts. The sparse activation of experts enables a significant reduction of the computational cost when training large-scale models. To further enhance computational efficiency, a TOP-K[37] sparse gating mechanism is employed, selecting only a subset of experts in each layer. This approach enables MoE models to scale linearly in size while maintaining manageable computational requirements, depending on the number of experts included in the weighted averaging. In contrast to the traditional Top-K mechanism, the Adaptive Expert Activation (AEA-MOE) mechanism proposed in this paper employs an adaptive routing algorithm that dynamically adjusts the number of activated experts based on the complexity of the input data, thereby enabling more efficient utilization of computational resources.

3 Proposed Method

3.1 Framework

The overall framework is illustrated in figure2. The framework contains four types of modal data: I_{rgb} , I_s , I_{ir} , and T , corresponding to RGB, sketch, infrared, and text, respectively. We employ CLIP (ViT-B/16) as the backbone of our network. Specifically, the Image encoder is used to extract features from the three image modalities, while the Text encoder is used to extract features from the text modality.

For the Image encoder, the image is first divided into N patches, which are then mapped into embedding vectors through linear projection, with positional information added to enhance spatial awareness. Subsequently, a [CLS] token is introduced at the beginning of the embedding vectors to represent the global features of the image. These $N+1$ tokens are then fed into a series of transformer blocks. In order to efficiently extract features of diverse modalities, the Adaptive Expert Allocation Mixture of Experts(AEA-MOE) mechanism is introduced. After processing through the multi-head attention mechanism, an adaptive routing algorithm is employed to dynamically select the experts to be activated based on the confidence level of each expert. Unlike the traditional Top-K routing mechanism that selects a fixed number of experts, the adaptive routing algorithm can dynamically adjust the number of activated experts based on the input feature attributes. Additionally, to ensure that the adaptive routing algorithm selects the smallest necessary set of experts, an adaptive loss is introduced.

For the Text encoder, the text description T is tokenized using a simple tokenizer with a vocabulary of 49,152 words, converting it into embedding vectors e . A [BOS] token is added at the beginning of the sequence as a start token, and an [EOS] token is added at the end as an end token. Thus, the

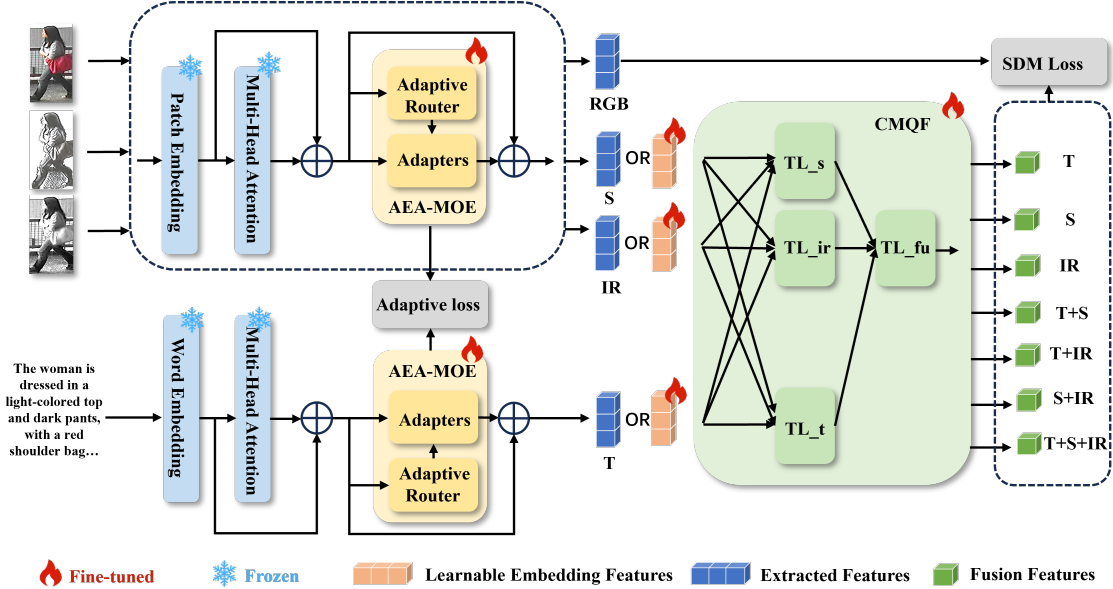


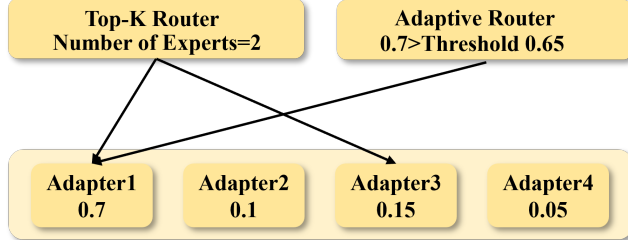
Figure 2: The network architecture of the proposed FlexiReID. All visual modalities share a single visual encoder. The incorporation of AEA-MOE facilitates the efficient processing of heterogeneous modality data. CMQF is employed to seamlessly integrate diverse modality features, while learnable embedding features are utilized to compensate for any missing modalities.

entire sequence can be represented as $\{e_{bos}, e_1, \dots, e_{eos}\}$, and is fed into the transformer blocks. The subsequent processing is similar to that of the Image encoder and will not be repeated here.

The final image feature representations are denoted as $\{v_{cls}^*, v_1^*, \dots, v_M^*\}$, and the text feature representations are denoted as $\{t_{bos}, t_1, \dots, t_{eos}\}$, where $*$ is used to indicate the three modalities within the image domain. Here, v_{cls}^* represents the global features of the image, and t_{eos} represents the global features of the text. Since FlexiReID supports seven retrieval strategies across four modalities, we propose a feature fusion module Cross-Modal Query Fusion(CMQF), which accepts multi-modal feature input, complements the missing modalities with learnable embedding features, and finally outputs seven fused features denoted as $\{f_s, fir, ft, fs_ir, fs_t, fir_t, fs_ir_t\}$. These seven fused features and visual representation v_{cls}^{rgb} are finally interacted and calculated by Similarity Distribution Matching (SDM) which is an effective matching loss function across different modalities.

To reduce the number of parameters during model training, we freeze the Patch Embedding, Word Embedding, and Multi-Head Attention components of the pre-trained model, and only train the Adaptive Expert Allocation Mixture of Experts(AEA-MOE), learnable embedding features and Cross-Modal Query Fusion(CMQF) modules.

Case 1: K=2 Threshold=0.65



Case 2: K=2 Threshold=0.65

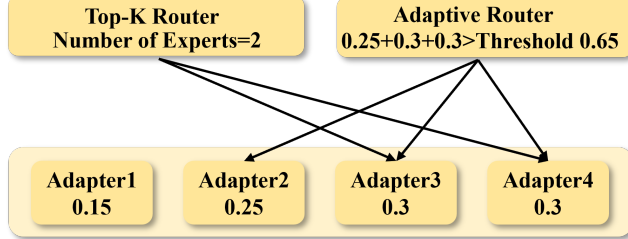


Figure 3: Traditional Top-K-based routing mechanisms are limited to selecting a fixed number of experts. In contrast, our proposed adaptive routing mechanism introduces a threshold confidence level, allowing the number of selected experts to be dynamically adjusted based on the input data.

3.2 Adaptive Expert Allocation Mixture of Experts (AEA-MOE)

In order to enhance the multimodal feature extraction capability of the model, we introduced the AEA-MOE mechanism. The traditional MOE based on Top-K routing calculates the confidence for each expert and activates the top K experts in confidence ranking. We argue that the activation strategy overlooks the diverse characteristics inherent in the input features. Different input features require the activation of different numbers of experts, and a fixed number of experts cannot meet the needs of extracting features from different modalities. Therefore, we propose an adaptive routing mechanism that dynamically selects the number of activated experts to extract features from different modalities. Specifically, we introduce a threshold confidence level. After the routing mechanism calculates the confidence level for each expert, it first compares the highest expert confidence level with the threshold. If the highest confidence level exceeds the threshold, only the corresponding expert is activated for feature extraction, and no additional experts are involved. If the highest confidence level does not exceed the threshold, experts are activated in descending order of confidence until the threshold is surpassed. This set of experts is then used for feature extraction. The data processing procedure of AEA-MOE can be formally represented as follows:

$$P = \text{Softmax}(W_r \cdot x^T) \quad (1)$$

$$g_i(\mathbf{x}) = \begin{cases} P_i, & Adapter_i \in S \\ 0, & Adapter_i \notin S \end{cases} \quad (2)$$

$$y = \sum_{i=1}^n g_i(x) Adapter_i(x) \quad (3)$$

where W_r represents the weights of the gating network within the routing mechanism, and P is a vector of size n , where P_i denotes the probability of selecting the i -th expert as computed by the gating network. S is the minimal set of experts whose confidence levels exceed the threshold. $g_i(x)$ indicates the probability of selecting the i -th expert as determined by the adaptive routing mechanism. Equation (3) illustrates the weighted summation process of experts and routing weights. The structure of the Adapter, inspired by [42], consists of a down-sampling layer, an intermediate activation layer, and an up-sampling layer.

To prevent the model from assigning small weights to each expert, resulting in the need to activate a large number of experts to exceed the threshold confidence level, which contradicts the principle of MOE to enhance computational efficiency and performance by activating only a few experts. We propose an adaptive loss to constrain the distribution of the probability P calculated by the gating function. We introduce the concept of entropy for adaptive loss calculation, formally expressed as follows:

$$\mathcal{L}_{ada} = - \sum_{i=1}^n P_i \log(P_i) \quad (4)$$

the adaptive loss ensures that the minimum necessary set of experts is activated, thereby enhancing computational efficiency. Simultaneously, it guarantees that the sum of the confidences of the activated experts exceeds the threshold confidence, and the activated experts can effectively extract features.

3.3 Cross-Modal Query Fusion (CMQF)

To effectively extract multimodal features and achieve flexible retrieval with various modality combinations, we propose the CMQF module. The features of the combined modalities are input into the CMQF module, and learnable embedded features are used to compensate for any missing modalities. Specifically, the features of each modality are input into their respective transformer blocks, where the query features are the sum of the query features from the other two modalities. Formally, this can be represented as:

$$\begin{aligned} y_s &= TL_s((X_{ir} + X_t)W_Q, X_sW_K, X_sW_V) \\ y_{ir} &= TL_ir((X_s + X_t)W_Q, X_{ir}W_K, X_{ir}W_V) \\ y_t &= TL_t((X_s + X_{ir})W_Q, X_tW_K, X_tW_V) \end{aligned} \quad (5)$$

Where X represents the input modality features, and W denotes the weight parameters used to generate the Query, Key, and Value. TL stands for the transformer block. Subsequently, all output features are concatenated and fed into a shared transformer block (TL_fu). Finally, the fused features are obtained through a mean pooling operation. This process can be formally represented as follows:

$$\begin{aligned} y &= \text{Concat}(y_s, y_{ir}, y_t) \\ f &= \text{MeanPool}(TL_fu(yW_Q, yW_K, yW_V)) \end{aligned} \quad (6)$$

After processing through the CMQF, we obtain seven types of modality-fused features: $\{f_s, f_{ir}, f_t, f_{s_ir}, f_{s_t}, f_{ir_t}\}$. These features correspond to the following modalities: sketch, infrared, text, sketch fused with infrared, sketch fused with text, infrared fused with text, and the fusion of sketch, infrared and text features.

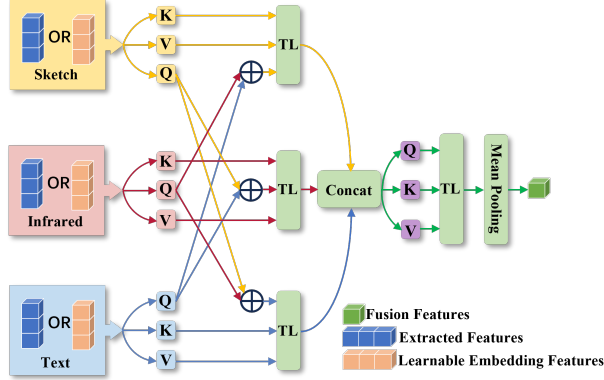


Figure 4: Our proposed CMQF Module.

3.4 Optimization and Inference

During the training phase, we utilize a parameter-free loss function called Similarity Distribution Matching (SDM)[43]. Jiang and Ye incorporate the cosine similarity distributions of the $N \times N$ embeddings for image-text pairs into the KL divergence to establish a connection between the two modalities. This is formally represented as:

$$\mathcal{L}_{i2t} = KL(\mathbf{p}_i || \mathbf{q}_i) = \frac{1}{N} \sum_{i=1}^N \sum_{j=1}^N p_{i,j} \log\left(\frac{p_{i,j}}{q_{i,j} + \epsilon}\right) \quad (7)$$

$$\mathcal{L}_{sdm} = \mathcal{L}_{i2t} + \mathcal{L}_{t2i} \quad (8)$$

where $p_{i,j}$ is the probability denoting the similarity between image-text pairs and $q_{i,j}$ is the true matching probability. \mathcal{L}_{sdm} is the bi-directional SDM loss.

Our model supports seven retrieval methods, each of which employs the SDM loss for its loss calculation. Therefore, the total loss is the aggregate of the SDM losses across all seven retrieval methods. Formally, this is expressed as:

$$\mathcal{L}_{sdm}^{sum} = \sum_{i=1}^7 \mathcal{L}_{sdm}^i \quad (9)$$

where \mathcal{L}_{sdm}^i denotes the SDM loss for the i -th retrieval method. Our framework is trained end-to-end, and the overall optimization objective is formally defined as:

$$\mathcal{L} = \mathcal{L}_{sdm}^{sum} + \lambda \mathcal{L}_{ada} \quad (10)$$

During inference, the trained network processes combinations of various modalities, assigning learnable Embedding Features to any missing modalities. It subsequently extracts integrated features across these modalities and computes their similarity with the RGB image embeddings. The Top-K candidates are then processed to derive the relevant evaluation metrics for each query.

4 Experiments

4.1 Experimental Setup

Datasets. In this study, we introduced four datasets: CUHK-PEDES, ICFG-PEDS, RSTPReid, and SYSU-MM01. To support the flexible retrieval capabilities of FlexiReid, which accommodates four modalities of pedestrian data, we expanded the modalities of these datasets. For the CUHK-PEDES, ICFG-PEDS, and RSTPReid datasets, which originally contain RGB images and textual descriptions, we employed StyleGAN3[44] to generate sketch modalities. This involved preprocessing each RGB image and using a pre-trained StyleGAN3 model to convert it into a sketch, preserving the primary contours and structural information of the original image. Concurrently, we used InfraGAN[45] to generate infrared image modalities. This was achieved by training the model on pairs of visible light and corresponding infrared images, and then applying the trained model to each RGB image to produce infrared images that capture thermal radiation information. For the SYSU-MM01 dataset, which originally contains RGB and infrared images, we similarly used StyleGAN3[44] to generate sketch modalities and employed the GPT-4 model to generate textual descriptions. This involved extracting features from each RGB image and generating corresponding textual descriptions that capture the main content and characteristics of the images. By incorporating these additional modalities, our expanded datasets better simulate real-world multimodal data scenarios, providing richer and more diverse data support for the training of the FlexiReid model. An overview of training and test set partitioning for each dataset can be found in the existing work[28, 24, 46].

Evaluation Protocols. Following existing cross-modality ReID settings[22, 23, 21], we use the Rank-k matching accuracy, mean Average Precision (mAP), and mean Inverse Negative Penalty (mINP)[21] metrics for performance evaluation in our FlexiReID.

Table 1: Comparison with the state-of-the-arts on CUHK-PEDES, ICFG-PEDES, and RSTPReid datasets. Rank (R) at k accuracy (%) is reported. The best results are bold.

Tasks	Methods	Venue	CUHK-PEDES					ICFG-PEDES					RSTPReid				
			R1	R5	R10	mAP	mINP	R1	R5	R10	mAP	mINP	R1	R5	R10	mAP	mINP
T→R	CMPM/C[47]	ECCV18	49.37	71.69	79.27	-	-	43.51	65.44	74.26	-	-	-	-	-	-	-
	MIA[48]	TIP20	-	-	-	-	-	46.49	67.14	75.18	-	-	-	-	-	-	-
	ViTAA[49]	ECCV20	55.97	75.84	83.52	-	-	50.98	68.79	75.78	-	-	-	-	-	-	-
	NAFS[29]	arXiv21	59.36	79.13	86.00	54.07	-	-	-	-	-	-	-	-	-	-	-
	DSSL[24]	MM21	59.98	80.41	87.56	-	-	-	-	-	-	-	32.43	55.08	63.19	-	-
	SSAN[28]	arXiv21	61.37	80.15	86.73	-	-	54.23	72.63	79.53	-	-	43.50	67.80	77.15	-	-
	Han et al.[50]	BMVC21	64.08	81.73	88.19	60.08	-	-	-	-	-	-	-	-	-	-	-
	LBUL+BERT[51]	MM22	64.04	82.66	87.22	-	-	-	-	-	-	-	45.55	68.20	77.85	-	-
	SAF[52]	ICASSP22	64.13	82.62	88.40	58.61	-	54.86	72.13	79.13	32.76	-	44.05	67.30	76.25	36.81	-
	TIPCB[53]	Neuro22	64.26	83.19	89.10	-	-	54.96	74.72	81.89	-	-	-	-	-	-	-
	CAIBC[54]	MM22	64.43	82.87	87.35	-	-	-	-	-	-	-	47.35	69.55	79.00	-	-
	AXM-Net[55]	MM22	64.44	80.52	86.77	58.73	-	-	-	-	-	-	-	-	-	-	-
	LGUR[30]	MM22	65.25	83.12	89.00	-	-	59.02	75.32	81.56	-	-	-	-	-	-	-
	IVT[56]	ECCV22	65.59	83.11	89.21	-	-	56.04	73.60	80.22	-	-	46.70	70.00	78.80	-	-
	UNIReID[57]	CVPR23	68.71	85.35	90.84	-	-	61.28	77.40	83.16	-	-	60.25	79.85	87.10	-	-
	CFine[58]	TIP23	69.57	85.93	91.15	-	-	60.83	76.55	82.42	-	-	50.55	72.50	81.60	-	-
	CSKT[59]	ICASSP24	69.70	86.92	91.80	62.74	-	58.90	77.31	83.56	33.87	-	57.75	81.30	88.35	46.43	-
	FlexiReID(Ours)	-	69.20	86.43	91.41	62.47	48.32	61.34	78.41	83.92	35.73	7.53	55.79	79.62	86.48	45.37	26.25
S→R	Sketch Trans+[60]	PAMI23	81.39	90.61	93.54	73.72	64.72	74.83	86.75	91.52	38.64	5.68	61.37	80.15	88.29	48.94	25.73
	DALNet[61]	AAAI2024	83.03	92.39	94.58	75.39	66.82	77.28	87.84	92.61	40.35	6.18	64.68	83.27	89.06	51.08	27.13
	UNIReID[57]	CVPR23	84.87	-	-	78.85	68.55	77.47	-	-	40.41	6.31	65.80	-	-	51.22	27.47
	FlexiReID(Ours)	-	84.92	93.17	95.02	79.21	68.83	79.28	89.69	93.37	41.21	6.85	66.79	84.52	90.39	52.72	28.36
T+S→R	UNIReID[57]	CVPR23	86.29	-	-	80.92	71.30	82.17	-	-	47.00	8.74	73.20	-	-	58.72	34.61
	FlexiReID(Ours)	-	87.47	94.51	96.14	82.43	72.96	83.82	93.49	95.63	47.81	9.03	76.10	89.74	94.31	64.73	41.24
IR→R	GUR[62]	ICCV23	82.06	91.72	93.95	75.84	66.86	80.31	90.89	92.78	44.36	6.90	73.42	86.29	91.35	60.43	38.52
	SDCL[63]	CVPR24	84.57	92.73	94.58	77.32	68.20	81.36	91.83	94.07	45.81	7.92	74.67	87.94	93.16	62.75	39.93
	FlexiReID(Ours)	-	85.26	93.25	95.31	79.43	69.39	82.03	92.19	94.27	46.76	8.47	75.36	88.71	93.27	63.22	40.82
T+IR→R	FlexiReID(Ours)	-	86.23	94.07	96.52	81.49	70.96	82.42	92.56	95.08	47.35	8.75	75.84	89.28	94.11	63.90	40.98
S+IR→R	FlexiReID(Ours)	-	85.97	93.52	95.89	81.02	69.68	82.57	92.74	95.28	47.43	8.93	75.94	89.47	94.23	64.59	41.18
T+S+IR→R	FlexiReID(Ours)	-	88.23	95.13	96.75	82.63	73.05	84.26	93.78	96.15	48.09	9.42	76.35	90.26	95.08	65.19	42.29

Implementation Details. We employ the Vision Transformer[64] as the visual modalities feature learning backbone, and the Transformer model[65] as the textual modality feature learning backbone. Both backbones have pre-trained parameters derived from CLIP[13]. During the training process, all parameters of the backbone networks are frozen. In a batch, we randomly select 64 identities, each containing a sketch, an infrared, a text, and an RGB sample. The image is resized to 384×128 , and the length of textual token sequence is 77. We train our FlexiReID model with the Adam optimizer for 60 epochs. And the initial learning rate is computed as 1e-5 and decayed by a cosine schedule. The threshold confidence level is set to 0.6, and the number of experts is 6. The hyperparameter λ that indicates the adaptive loss is set to 0.5. We perform experiments on a single NVIDIA 3090 24GB GPU.

4.2 Performance Comparison

Results on CUHK-PEDES, ICFG-PEDES and RSTPReid In our experiments, we evaluated the model’s performance across seven different test tasks: $T \rightarrow R$, $S \rightarrow R$, $IR \rightarrow R$, $T + S \rightarrow R$, $T + IR \rightarrow R$, $S + IR \rightarrow R$, and $T + S + IR \rightarrow R$. The results, as shown in table 1, demonstrate the model’s performance on the CHUK-PEDES, ICFG-PEDES, and RSTPReid datasets. In the $T \rightarrow R$ task, our model achieved a Rank-K accuracy of 69.20% at R@1, 86.43% at R@5, and 91.41% at R@10

on the CHUK-PEDES dataset. On the ICFG-PEDES dataset, the model recorded a Rank-K accuracy of 61.34% at R@1, 78.41% at R@5, and 83.92% at R@10. For the RSTPReid dataset, the Rank-K accuracy was 55.79% at R@1, 79.62% at R@5, and 86.48% at R@10. Notably, the model achieved state-of-the-art (SOTA) performance on the ICFG-PEDES dataset and demonstrated performance close to SOTA on the CHUK-PEDES and RSTPReid datasets. These results underscore the model’s robust capability in text-to-image retrieval tasks. In the S→R task, our model achieved MAP metrics of 79.21%, 41.21%, and 52.72% on the three datasets, respectively. These results represent state-of-the-art (SOTA) performance across all datasets.

In other tasks ($T + S \rightarrow R$, $T + IR \rightarrow R$, $S + IR \rightarrow R$, $T + S + IR \rightarrow R$), our model also demonstrated robust performance. Compared to single-modality retrieval methods, the flexible combination of different modalities consistently achieved superior results. For instance, in the T+S+IR→R task, our model achieved Rank-K metrics of 88.23% at R@1, 95.13% at R@5, and 96.75% at R@10 on the CUHK-PEDES dataset, surpassing single-modality retrieval methods. This indicates that combining various modalities provides richer pedestrian detail information, thereby enhancing overall retrieval performance.

Overall, most current cross-modal ReID methods focus on retrieving RGB modality from a non-RGB modality. Our approach not only achieves state-of-the-art (SOTA) or near-SOTA performance in single-modality retrieval tasks but also supports a broader range of retrieval methods. The flexible combination of various modalities outperforms single-modality cross-modal retrieval methods, making our approach more versatile and widely applicable.

Table 2: Comparison with the state-of-the-arts on SYSU-MM01 datasets. Rank (R) at k accuracy (%) is reported. The best results are bold.

Tasks	Methods	Venue	All-Search				Indoor-Search			
			R1	R10	R20	mAP	R1	R10	R20	mAP
IR→R	SSFT[66]	CVPR20	61.6	89.2	93.9	63.3	70.5	94.9	97.7	72.6
	DDAG[67]	ECCV20	54.8	90.4	95.8	53.0	61.0	94.1	98.4	68.0
	DG-VAE[68]	MM20	59.5	93.8	-	58.5	-	-	-	-
	CICL+LAMA[69]	AAAI21	57.2	94.3	98.4	59.3	66.6	98.8	99.7	74.7
	VCD+VML[70]	CVPR21	60.0	94.2	98.1	58.8	66.1	96.6	99.4	73.0
	MPANet[71]	CVPR21	70.6	96.2	98.8	68.2	76.7	98.2	99.6	81.0
	MCLNet[72]	ICCV21	65.4	93.3	97.1	62.0	72.6	97.0	99.2	76.6
	SMCL[73]	ICCV21	67.4	92.9	96.8	61.8	68.8	96.6	98.8	75.6
	FlexiReID(Ours)	-	67.9	93.4	97.6	62.5	69.2	97.2	99.1	75.8
T→R	UNIReID[57]	CVPR23	54.3	90.2	95.7	63.8	56.7	91.8	96.5	66.9
	FlexiReID(Ours)	-	56.8	92.7	96.3	65.4	58.2	93.3	97.4	67.6
S→R	UNIReID[57]	CVPR23	64.7	90.9	94.6	59.2	66.7	95.4	97.8	74.0
	FlexiReID(Ours)	-	66.4	92.7	95.2	60.3	68.5	96.7	98.2	75.3
T+S→R	UNIReID[57]	CVPR23	66.5	94.2	97.9	66.4	69.3	94.6	97.5	72.8
	FlexiReID(Ours)	-	68.7	95.1	98.3	67.2	70.6	95.0	97.9	73.4
T+IR→R	FlexiReID(Ours)	-	68.9	96.7	98.2	68.1	71.2	98.3	99.3	75.2
	FlexiReID(Ours)	-	69.0	96.4	98.5	68.6	72.2	98.7	99.4	76.2
T+S+IR→R	FlexiReID(Ours)	-	71.3	97.2	98.7	69.5	73.2	98.9	99.6	77.3

Results on SYSU-MM01 We also evaluated our model on the SYSU-MM01 dataset, as shown in table 2. In the IR → RGB task under the full search mode, our model demonstrated competitive performance, approaching the state-of-the-art (SOTA) level. However, by flexibly combining other modalities, performance can be further enhanced. For instance, in the Indoor-Search mode for the $T + S + IR \rightarrow R$ task, our model achieved Rank-K metrics of 73.2% on R@1, 98.9% on R@10, and

99.6% on R@20. This improvement is attributed to the introduction of text and sketch modalities, which provide additional pedestrian features and enhance the model’s comprehension capabilities.

Table 3: Ablation study on R@1 about each component of FlexiReID. The metric Avg. denotes the average R@1 across seven search modes.

No.	Module	Components				$T \rightarrow R$	$S \rightarrow R$	$IR \rightarrow R$	$T + S \rightarrow R$	$T + IR \rightarrow R$	$S + IR \rightarrow R$	$T + S + IR \rightarrow R$	Avg.
		MLP-Adapter	AEA-MOE	AL	CMQF								
0	Zero-shot CLIP					12.58	2.47	3.79	1.62	2.73	3.72	4.51	4.49
1	+MLP-Adapter	✓				66.38	81.47	81.93	83.58	83.26	82.43	85.03	80.58
2	+AEA-MOE(w/o AL)	✓	✓			68.45	83.08	83.74	85.83	85.52	84.32	86.71	82.52
3	+AEA-MOE(w/ AL)	✓	✓	✓		68.87	84.13	84.37	86.41	85.93	84.97	87.35	83.14
4	+CMQF(w/o LEF)	✓	✓	✓	✓	69.08	84.59	85.12	87.38	86.15	85.78	88.05	83.73
5	+CMQF(w/ LEF)	✓	✓	✓	✓	69.20	84.92	85.26	87.47	86.23	85.97	88.23	83.90

4.3 Ablation Study

A comprehensive ablation study for components of FlexiReID is presented in Table 3, including the most critical accuracy metric R@1 and the average metric on CUHKPEDES datasets. The results in No.0 serve as the backbone baseline by zero-shot CLIP, where inference is performed directly on the original frozen CLIP model without adding any additional trainable modules. No.1 employs the traditional MOE method, while No.2 and No.3 utilize AEA-MOE. It is evident that AEA-MOE outperforms the traditional MOE in handling data from various modalities, thereby achieving superior performance. Furthermore, incorporating adaptive loss further enhances performance. As demonstrated by No.4, CMQF plays a pivotal role in the integration of features from different modalities, thereby improving the model’s performance. Moreover, substituting missing modalities with Learnable Embedding Features yields optimal performance. These results indicate that each component of FlexiReID significantly contributes to the model’s overall performance, working in concert to achieve optimal outcomes.

Ablation Study on Routing Strategies To evaluate the effectiveness of our proposed adaptive routing mechanism, we conduct a comprehensive ablation study by comparing it with several widely adopted routing strategies, including Top-K routing, soft routing, and hash routing. As shown in Table 4, our adaptive routing achieves the best overall performance. These results demonstrate that our method benefits from dynamically selecting both the number and combination of experts based on the input features, rather than relying on fixed or probabilistic routing strategies. This ablation study highlights the critical role of adaptive expert allocation in enhancing feature expressiveness and improving downstream retrieval performance.

Ablation Study on Feature Fusion Strategies To validate the effectiveness of the proposed Cross-Modal Query Fusion (CMQF) module, we conducted an ablation study comparing it with several commonly used multimodal feature fusion strategies, including concatenation, summation, and hierarchical fusion. Specifically, the concatenation strategy directly concatenates features from different modalities and feeds them into a shared Transformer for fusion. The summation strategy aggregates features by summing them prior to Transformer processing. The hierarchical fusion ap-

Table 4: Comparison of different routing strategies.

Method	Avg.
Top-K Routing	80.58
Soft Routing	81.80
Hash Routing	83.11
Ours (Adaptive Routing)	83.90

proach first encodes each modality independently using separate Transformers and then performs fusion at a shared layer. All methods were evaluated on the modality-augmented CUHK-PEDES dataset, and the average R@1 accuracy across seven retrieval tasks was reported. As shown in Table 5, CMQF achieved the best overall performance. Compared to the aforementioned methods, CMQF leverages cross-modal attention mechanisms and incorporates learnable embedding features to compensate for missing modalities, enabling more comprehensive and robust feature alignment. These results demonstrate the superior capability of CMQF in enhancing multimodal feature representations and improving retrieval accuracy.

Table 5: Comparison of different feature fusion strategies

Method	Avg.
Concatenation	83.14
Summation	82.24
Hierarchical Fusion	83.51
CMQF (Ours)	83.90

4.4 Hyper-Parameter Analysis

The Number of Experts. As shown in Figure 5a, to investigate the impact of the number of experts n , we sample n as 2, 4, 6, 8 and 10, to evaluate the R@1 accuracy and mAP under different numbers of experts. A constant threshold confidence level is fixed to 0.4 in the overall experiment. When n is less than 6, average R@1 performance gradually increases with an increasing number of experts. However, when n exceeds 6, larger n leads to a decrease in performance. we observe that although increasing n can proportionally enhance the model’s information capacity, a larger n does not necessarily lead to better performance. This suggests that the model’s capacity cannot grow indefinitely. We ultimately determine $n = 6$ as a practical choice.

Threshold Confidence Level As shown in Figure 5b, we set the number of experts $n = 6$ and explore the R@1 accuracy and mAP with the change of threshold confidence level. When the confidence level is low, the model’s performance is poor. However, as the threshold confidence level increases to 0.4, the performance reaches its peak. As the threshold confidence level increases further, the model’s

performance essentially reaches a plateau without additional improvement. Therefore, the threshold confidence level is set to 0.4.

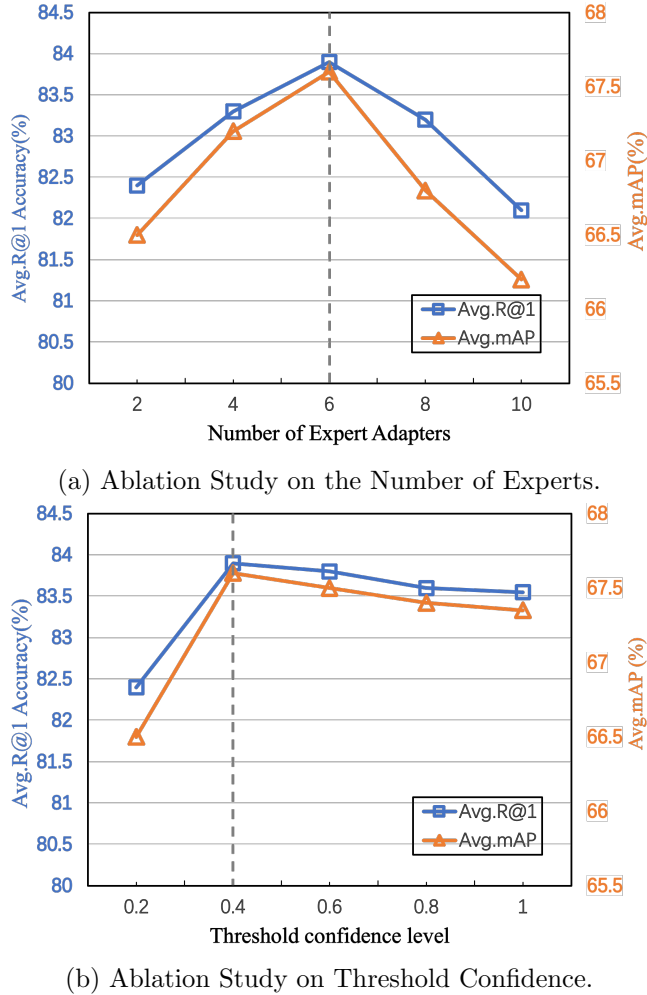


Figure 5: Ablation Study on the Number of Experts and Threshold Confidence.

5 Conclusion

In this paper, we propose FlexiReID, a multimodal person re-identification framework that supports flexible retrieval across four modalities: text, sketches, RGB, and infrared, as well as any combination thereof. We design the AEA-MoE mechanism to dynamically select expert networks and introduce the CMQF module to optimize cross-modal feature fusion. Based on the expanded CIRS-PEDES dataset, experimental results demonstrate that FlexiReID outperforms existing methods in complex scenarios, validating its flexibility and effectiveness, and opening up new research directions for multimodal person re-identification.

References

- [1] Kaiyang Zhou, Jingkang Yang, Chen Change Loy, and Ziwei Liu. Learning to prompt for vision-language models. *International Journal of Computer Vision*, 130(9):2337–2348, 2022.
- [2] Peng Gao, Shijie Geng, Renrui Zhang, Teli Ma, Rongyao Fang, Yongfeng Zhang, Hongsheng Li, and Yu Qiao. Clip-adapter: Better vision-language models with feature adapters. *International Journal of Computer Vision*, 132(2):581–595, 2024.
- [3] Tao Yu, Zhihe Lu, Xin Jin, Zhibo Chen, and Xinchao Wang. Task residual for tuning vision-language models. In *Proceedings of the IEEE/CVF Conference on Computer Vision and Pattern Recognition*, pages 10899–10909, 2023.
- [4] Alex Nichol, Prafulla Dhariwal, Aditya Ramesh, Pranav Shyam, Pamela Mishkin, Bob McGrew, Ilya Sutskever, and Mark Chen. Glide: Towards photorealistic image generation and editing with text-guided diffusion models. *arXiv preprint arXiv:2112.10741*, 2021.
- [5] Aditya Ramesh, Prafulla Dhariwal, Alex Nichol, Casey Chu, and Mark Chen. Hierarchical text-conditional image generation with clip latents. *arXiv preprint arXiv:2204.06125*, 1(2):3, 2022.
- [6] Or Patashnik, Zongze Wu, Eli Shechtman, Daniel Cohen-Or, and Dani Lischinski. Styleclip: Text-driven manipulation of stylegan imagery. In *Proceedings of the IEEE/CVF international conference on computer vision*, pages 2085–2094, 2021.
- [7] Hongwei Niu, Linhuang Xie, Jianghang Lin, and Shengchuan Zhang. Exploring semantic consistency and style diversity for domain generalized semantic segmentation. In *Proceedings of the AAAI Conference on Artificial Intelligence*, volume 39, pages 6245–6253, 2025.
- [8] Mengmeng Wang, Jiazheng Xing, and Yong Liu. Actionclip: A new paradigm for video action recognition. *arXiv preprint arXiv:2109.08472*, 2021.
- [9] Jiasen Lu, Dhruv Batra, Devi Parikh, and Stefan Lee. Vilbert: Pretraining task-agnostic visiolinguistic representations for vision-and-language tasks. *Advances in neural information processing systems*, 32, 2019.
- [10] Weijie Su, Xizhou Zhu, Yue Cao, Bin Li, Lewei Lu, Furu Wei, and Jifeng Dai. Vl-bert: Pre-training of generic visual-linguistic representations. *arXiv preprint arXiv:1908.08530*, 2019.
- [11] Hao Tan and Mohit Bansal. Lxmert: Learning cross-modality encoder representations from transformers. *arXiv preprint arXiv:1908.07490*, 2019.
- [12] Yen-Chun Chen, Linjie Li, Licheng Yu, Ahmed El Kholy, Faisal Ahmed, Zhe Gan, Yu Cheng, and Jingjing Liu. Uniter: Universal image-text representation learning. In *European conference on computer vision*, pages 104–120. Springer, 2020.

- [13] Alec Radford, Jong Wook Kim, Chris Hallacy, Aditya Ramesh, Gabriel Goh, Sandhini Agarwal, Girish Sastry, Amanda Askell, Pamela Mishkin, Jack Clark, et al. Learning transferable visual models from natural language supervision. In *International conference on machine learning*, pages 8748–8763. PMLR, 2021.
- [14] Chao Jia, Yafei Yang, Ye Xia, Yi-Ting Chen, Zarana Parekh, Hieu Pham, Quoc Le, Yun-Hsuan Sung, Zhen Li, and Tom Duerig. Scaling up visual and vision-language representation learning with noisy text supervision. In *International conference on machine learning*, pages 4904–4916. PMLR, 2021.
- [15] Junnan Li, Ramprasaath Selvaraju, Akhilesh Gotmare, Shafiq Joty, Caiming Xiong, and Steven Chu Hong Hoi. Align before fuse: Vision and language representation learning with momentum distillation. *Advances in neural information processing systems*, 34:9694–9705, 2021.
- [16] Xiaohua Zhai, Xiao Wang, Basil Mustafa, Andreas Steiner, Daniel Keysers, Alexander Kolesnikov, and Lucas Beyer. Lit: Zero-shot transfer with locked-image text tuning. In *Proceedings of the IEEE/CVF conference on computer vision and pattern recognition*, pages 18123–18133, 2022.
- [17] Hongwei Niu, Jie Hu, Jianghang Lin, Guannan Jiang, and Shengchuan Zhang. Eov-seg: Efficient open-vocabulary panoptic segmentation. In *Proceedings of the AAAI Conference on Artificial Intelligence*, volume 39, pages 6254–6262, 2025.
- [18] Jaemin Cho, Jie Lei, Hao Tan, and Mohit Bansal. Unifying vision-and-language tasks via text generation. In *International Conference on Machine Learning*, pages 1931–1942. PMLR, 2021.
- [19] Aditya Ramesh, Mikhail Pavlov, Gabriel Goh, Scott Gray, Chelsea Voss, Alec Radford, Mark Chen, and Ilya Sutskever. Zero-shot text-to-image generation. In *International conference on machine learning*, pages 8821–8831. Pmlr, 2021.
- [20] Cuiqun Chen, Mang Ye, Meibin Qi, Jingjing Wu, Yimin Liu, and Jianguo Jiang. Saliency and granularity: Discovering temporal coherence for video-based person re-identification. *IEEE Transactions on Circuits and Systems for Video Technology*, 32(9):6100–6112, 2022.
- [21] Mang Ye, Jianbing Shen, Gaojie Lin, Tao Xiang, Ling Shao, and Steven CH Hoi. Deep learning for person re-identification: A survey and outlook. *IEEE transactions on pattern analysis and machine intelligence*, 44(6):2872–2893, 2021.
- [22] Cuiqun Chen, Mang Ye, Meibin Qi, and Bo Du. Sketch transformer: Asymmetrical disentanglement learning from dynamic synthesis. In *Proceedings of the 30th ACM International Conference on Multimedia*, pages 4012–4020, 2022.

- [23] Mang Ye, Weijian Ruan, Bo Du, and Mike Zheng Shou. Channel augmented joint learning for visible-infrared recognition. In *Proceedings of the IEEE/CVF International Conference on Computer Vision*, pages 13567–13576, 2021.
- [24] Aichun Zhu, Zijie Wang, Yifeng Li, Xili Wan, Jing Jin, Tian Wang, Fangqiang Hu, and Gang Hua. Dssl: Deep surroundings-person separation learning for text-based person retrieval. In *Proceedings of the 29th ACM international conference on multimedia*, pages 209–217, 2021.
- [25] Cuiqun Chen, Mang Ye, Meibin Qi, Jingjing Wu, Jianguo Jiang, and Chia-Wen Lin. Structure-aware positional transformer for visible-infrared person re-identification. *IEEE Transactions on Image Processing*, 31:2352–2364, 2022.
- [26] Bin Yang, Mang Ye, Jun Chen, and Zesen Wu. Augmented dual-contrastive aggregation learning for unsupervised visible-infrared person re-identification. In *Proceedings of the 30th ACM International Conference on Multimedia*, pages 2843–2851, 2022.
- [27] Mang Ye, Cuiqun Chen, Jianbing Shen, and Ling Shao. Dynamic tri-level relation mining with attentive graph for visible infrared re-identification. *IEEE Transactions on Information Forensics and Security*, 17:386–398, 2021.
- [28] Zefeng Ding, Changxing Ding, Zhiyin Shao, and Dacheng Tao. Semantically self-aligned network for text-to-image part-aware person re-identification. *arXiv preprint arXiv:2107.12666*, 2021.
- [29] Chenyang Gao, Guanyu Cai, Xinyang Jiang, Feng Zheng, Jun Zhang, Yifei Gong, Pai Peng, Xiaowei Guo, and Xing Sun. Contextual non-local alignment over full-scale representation for text-based person search. *arXiv preprint arXiv:2101.03036*, 2021.
- [30] Zhiyin Shao, Xinyu Zhang, Meng Fang, Zhifeng Lin, Jian Wang, and Changxing Ding. Learning granularity-unified representations for text-to-image person re-identification. In *Proceedings of the 30th ACM international conference on multimedia*, pages 5566–5574, 2022.
- [31] Shaojun Gui, Yu Zhu, Xiangxiang Qin, and Xiaofeng Ling. Learning multi-level domain invariant features for sketch re-identification. *Neurocomputing*, 403:294–303, 2020.
- [32] Fan Yang, Yang Wu, Zheng Wang, Xiang Li, Sakriani Sakti, and Satoshi Nakamura. Instance-level heterogeneous domain adaptation for limited-labeled sketch-to-photo retrieval. *IEEE Transactions on Multimedia*, 23:2347–2360, 2020.
- [33] Shuang Li, Tong Xiao, Hongsheng Li, Bolei Zhou, Dayu Yue, and Xiaogang Wang. Person search with natural language description. In *Proceedings of the IEEE conference on computer vision and pattern recognition*, pages 1970–1979, 2017.
- [34] Lu Pang, Yaowei Wang, Yi-Zhe Song, Tiejun Huang, and Yonghong Tian. Cross-domain adversarial feature learning for sketch re-identification. In *Proceedings of the 26th ACM international conference on Multimedia*, pages 609–617, 2018.

[35] Yajing Zhai, Yawen Zeng, Da Cao, and Shaofei Lu. Trireid: Towards multi-modal person re-identification via descriptive fusion model. In *Proceedings of the 2022 International Conference on Multimedia Retrieval*, pages 63–71, 2022.

[36] Carlos Riquelme, Joan Puigcerver, Basil Mustafa, Maxim Neumann, Rodolphe Jenatton, André Susano Pinto, Daniel Keysers, and Neil Houlsby. Scaling vision with sparse mixture of experts. *Advances in Neural Information Processing Systems*, 34:8583–8595, 2021.

[37] Noam Shazeer, Azalia Mirhoseini, Krzysztof Maziarz, Andy Davis, Quoc Le, Geoffrey Hinton, and Jeff Dean. Outrageously large neural networks: The sparsely-gated mixture-of-experts layer. *arXiv preprint arXiv:1701.06538*, 2017.

[38] Junyi Chen, Longteng Guo, Jia Sun, Shuai Shao, Zehuan Yuan, Liang Lin, and Dongyu Zhang. Eve: Efficient vision-language pre-training with masked prediction and modality-aware moe. In *Proceedings of the AAAI Conference on Artificial Intelligence*, volume 38, pages 1110–1119, 2024.

[39] David Eigen, Marc’Aurelio Ranzato, and Ilya Sutskever. Learning factored representations in a deep mixture of experts. *arXiv preprint arXiv:1312.4314*, 2013.

[40] William Fedus, Barret Zoph, and Noam Shazeer. Switch transformers: Scaling to trillion parameter models with simple and efficient sparsity. *Journal of Machine Learning Research*, 23(120):1–39, 2022.

[41] Dmitry Lepikhin, HyoukJoong Lee, Yuanzhong Xu, Dehao Chen, Orhan Firat, Yanping Huang, Maxim Krikun, Noam Shazeer, and Zhifeng Chen. Gshard: Scaling giant models with conditional computation and automatic sharding. *arXiv preprint arXiv:2006.16668*, 2020.

[42] Shoufa Chen, Chongjian Ge, Zhan Tong, Jiangliu Wang, Yibing Song, Jue Wang, and Ping Luo. Adaptformer: Adapting vision transformers for scalable visual recognition. *Advances in Neural Information Processing Systems*, 35:16664–16678, 2022.

[43] Ding Jiang and Mang Ye. Cross-modal implicit relation reasoning and aligning for text-to-image person retrieval. In *Proceedings of the IEEE/CVF Conference on Computer Vision and Pattern Recognition*, pages 2787–2797, 2023.

[44] Tero Karras, Miika Aittala, Samuli Laine, Erik Härkönen, Janne Hellsten, Jaakko Lehtinen, and Timo Aila. Alias-free generative adversarial networks. *Advances in neural information processing systems*, 34:852–863, 2021.

[45] Mehmet Akif Özkanoglu and Sedat Ozer. Infragan: A gan architecture to transfer visible images to infrared domain. *Pattern Recognition Letters*, 155:69–76, 2022.

[46] Ancong Wu, Wei-Shi Zheng, Shaogang Gong, and Jianhuang Lai. Rgb-ir person re-identification by cross-modality similarity preservation. *International journal of computer vision*, 128(6):1765–1785, 2020.

[47] Ying Zhang and Huchuan Lu. Deep cross-modal projection learning for image-text matching. In *Proceedings of the European conference on computer vision (ECCV)*, pages 686–701, 2018.

[48] Kai Niu, Yan Huang, Wanli Ouyang, and Liang Wang. Improving description-based person re-identification by multi-granularity image-text alignments. *IEEE Transactions on Image Processing*, 29:5542–5556, 2020.

[49] Zhe Wang, Zhiyuan Fang, Jun Wang, and Yezhou Yang. Vitaa: Visual-textual attributes alignment in person search by natural language. In *Computer Vision–ECCV 2020: 16th European Conference, Glasgow, UK, August 23–28, 2020, Proceedings, Part XII 16*, pages 402–420. Springer, 2020.

[50] Xiao Han, Sen He, Li Zhang, and Tao Xiang. Text-based person search with limited data. *arXiv preprint arXiv:2110.10807*, 2021.

[51] Zijie Wang, Aichun Zhu, Jingyi Xue, Xili Wan, Chao Liu, Tian Wang, and Yifeng Li. Look before you leap: Improving text-based person retrieval by learning a consistent cross-modal common manifold. In *Proceedings of the 30th ACM international conference on multimedia*, pages 1984–1992, 2022.

[52] Shiping Li, Min Cao, and Min Zhang. Learning semantic-aligned feature representation for text-based person search. In *ICASSP 2022-2022 IEEE International Conference on Acoustics, Speech and Signal Processing (ICASSP)*, pages 2724–2728. IEEE, 2022.

[53] Yuhao Chen, Guoqing Zhang, Yujiang Lu, Zhenxing Wang, and Yuhui Zheng. Tipcb: A simple but effective part-based convolutional baseline for text-based person search. *Neurocomputing*, 494:171–181, 2022.

[54] Zijie Wang, Aichun Zhu, Jingyi Xue, Xili Wan, Chao Liu, Tian Wang, and Yifeng Li. Caibc: Capturing all-round information beyond color for text-based person retrieval. In *Proceedings of the 30th ACM international conference on multimedia*, pages 5314–5322, 2022.

[55] Ammarah Farooq, Muhammad Awais, Josef Kittler, and Syed Safwan Khalid. Axm-net: Implicit cross-modal feature alignment for person re-identification. In *Proceedings of the AAAI conference on artificial intelligence*, volume 36, pages 4477–4485, 2022.

[56] Xiujun Shu, Wei Wen, Haoqian Wu, Keyu Chen, Yiran Song, Ruizhi Qiao, Bo Ren, and Xiao Wang. See finer, see more: Implicit modality alignment for text-based person retrieval. In *European Conference on Computer Vision*, pages 624–641. Springer, 2022.

[57] Cuiqun Chen, Mang Ye, and Ding Jiang. Towards modality-agnostic person re-identification with descriptive query. In *Proceedings of the IEEE/CVF Conference on Computer Vision and Pattern Recognition*, pages 15128–15137, 2023.

[58] Shuanglin Yan, Neng Dong, Liyan Zhang, and Jinhui Tang. Clip-driven fine-grained text-image person re-identification. *IEEE Transactions on Image Processing*, 2023.

[59] Yating Liu, Yaowei Li, Zimo Liu, Wenming Yang, Yaowei Wang, and Qingmin Liao. Clip-based synergistic knowledge transfer for text-based person retrieval. In *ICASSP 2024-2024 IEEE International Conference on Acoustics, Speech and Signal Processing (ICASSP)*, pages 7935–7939. IEEE, 2024.

[60] Cuiqun Chen, Mang Ye, Meibin Qi, and Bo Du. Sketchtrans: Disentangled prototype learning with transformer for sketch-photo recognition. *IEEE Transactions on Pattern Analysis and Machine Intelligence*, 46(5):2950–2964, 2023.

[61] Xingyu Liu, Xu Cheng, Haoyu Chen, Hao Yu, and Guoying Zhao. Differentiable auxiliary learning for sketch re-identification. In *Proceedings of the AAAI Conference on Artificial Intelligence*, volume 38, pages 3747–3755, 2024.

[62] Bin Yang, Jun Chen, and Mang Ye. Towards grand unified representation learning for unsupervised visible-infrared person re-identification. In *Proceedings of the IEEE/CVF International Conference on Computer Vision*, pages 11069–11079, 2023.

[63] Bin Yang, Jun Chen, and Mang Ye. Shallow-deep collaborative learning for unsupervised visible-infrared person re-identification. In *Proceedings of the IEEE/CVF Conference on Computer Vision and Pattern Recognition*, pages 16870–16879, 2024.

[64] Alexey Dosovitskiy. An image is worth 16x16 words: Transformers for image recognition at scale. *arXiv preprint arXiv:2010.11929*, 2020.

[65] A Vaswani. Attention is all you need. *Advances in Neural Information Processing Systems*, 2017.

[66] Yan Lu, Yue Wu, Bin Liu, Tianzhu Zhang, Baopu Li, Qi Chu, and Nenghai Yu. Cross-modality person re-identification with shared-specific feature transfer. In *Proceedings of the IEEE/CVF conference on computer vision and pattern recognition*, pages 13379–13389, 2020.

[67] Mang Ye, Jianbing Shen, David J. Crandall, Ling Shao, and Jiebo Luo. Dynamic dual-attentive aggregation learning for visible-infrared person re-identification. In *Computer Vision–ECCV 2020: 16th European Conference, Glasgow, UK, August 23–28, 2020, Proceedings, Part XVII 16*, pages 229–247. Springer, 2020.

[68] Nan Pu, Wei Chen, Yu Liu, Erwin M Bakker, and Michael S Lew. Dual gaussian-based variational subspace disentanglement for visible-infrared person re-identification. In *Proceedings of the 28th ACM international conference on multimedia*, pages 2149–2158, 2020.

- [69] Zhiwei Zhao, Bin Liu, Qi Chu, Yan Lu, and Nenghai Yu. Joint color-irrelevant consistency learning and identity-aware modality adaptation for visible-infrared cross modality person re-identification. In *Proceedings of the AAAI conference on artificial intelligence*, volume 35, pages 3520–3528, 2021.
- [70] Xudong Tian, Zhizhong Zhang, Shaohui Lin, Yanyun Qu, Yuan Xie, and Lizhuang Ma. Farewell to mutual information: Variational distillation for cross-modal person re-identification. In *Proceedings of the IEEE/CVF Conference on Computer Vision and Pattern Recognition*, pages 1522–1531, 2021.
- [71] Qiong Wu, Pingyang Dai, Jie Chen, Chia-Wen Lin, Yongjian Wu, Feiyue Huang, Bineng Zhong, and Rongrong Ji. Discover cross-modality nuances for visible-infrared person re-identification. In *Proceedings of the IEEE/CVF conference on computer vision and pattern recognition*, pages 4330–4339, 2021.
- [72] Xin Hao, Sanyuan Zhao, Mang Ye, and Jianbing Shen. Cross-modality person re-identification via modality confusion and center aggregation. In *Proceedings of the IEEE/CVF International conference on computer vision*, pages 16403–16412, 2021.
- [73] Ziyu Wei, Xi Yang, Nannan Wang, and Xinbo Gao. Syncretic modality collaborative learning for visible infrared person re-identification. In *Proceedings of the IEEE/CVF international conference on computer vision*, pages 225–234, 2021.